

High Temperature Corrosion Behavior of Superficially Applied CeO₂ on Some Fe-, Co- and Ni-Based Superalloys

Gitanjali^a, N. Bala^b, H. Singh^c and S. Prakash^d

^a*Metallurgical and Materials Engineering Department,
National Institute of Technology Srinagar (J&K), India,
e-mail: gitagoyal@rediffmail.com*

^b*Baba Banda Singh Bahadur Engineering College,
Fatehgarh Sahib, Punjab, India, e-mail: nirajbala@gmail.com*

^c*Indian Institute of Technology Ropar,
Rupnagar, Punjab, India, e-mail: harpreetsingh@iitrpr.ac.in*

^d*Indian Institute of Technology Roorkee,
Roorkee, Uttarakhand, India, e-mail: truthfmt@iitr.ernet.in*

High temperature corrosion of metals and alloys can be controlled by the use of inhibitors. In this work, the role of a superficially applied CeO₂ coating to combat high temperature corrosion of some superalloys such as Superfer 800H (Alloy A), Superco 605 (Alloy B) and Superni 75 (Alloy C) has been investigated. An accelerated corrosion testing of the coated as well as bare superalloys was done in a molten salt environment (Na₂SO₄-60% V₂O₅) at 900°C for 50 cycles. The weight change, X-ray diffraction (XRD), Scanning Electron Microscopy (SEM) and Electron Probe Micro-Analysis (EPMA) of the exposed specimens were carried out to characterize the oxide scales. The percentage decrease in the weight gain in alloys A, B and C, with superficially applied CeO₂, was found to be 23, 35 and 68%, respectively. It was concluded that ceria (ceric oxide) was most effective in reducing the corrosion rate in alloy C.

Keywords: superalloys, hot corrosion, inhibitors, oxide additives.

УДК 620:22

INTRODUCTION

Metals, alloys, and ceramics may sometimes experience accelerated oxidation when their surfaces are covered with a thin film of a fused salt in an oxidizing atmosphere at elevated temperatures. This mode of attack is called hot corrosion or high temperature corrosion. High temperature corrosion can be defined as the deposit modified gas-induced degradation of materials at high temperatures [1].

Many very important engineering systems operating at high temperatures (650–1100°C) involve a contact of metallic or ceramic materials with combustion gases containing inorganic impurities, e.g. gas turbines, steam generators, incinerators and numerous petrochemical process vessels. As the gases are cooled, fused salt films may condense on the hardware to generate a highly corrosive condition analogous to the aqueous atmospheric corrosion resulting in an accelerated degradation [2]. “Because of its high thermodynamic stability in the mutual presence of sodium and sulphur impurities in the oxidizing gas, Na₂SO₄ is often found to be the common or dominant component of the salt deposit. Sulphur is a principal impurity in fossil fuels, and sodium is introduced into the combustion air – usually in an aerosol originating from seawater.” [1] “During the combustion of certain low-grade fossil fuels, vanadium compounds such as NaVO₃ and V₂O₅, may also be deposited in the salt film” [1].

Iron, nickel- and cobalt-based superalloys are commercial alloys commonly used for the manufacture of components exploited in aggressive environments of gas turbines, steam boilers etc, where these

alloys are subject to the hot corrosion degradation. There are numerous inhibitors commercially available that are intended to reduce the severity of oil ash corrosion (hot corrosion), such as Mg- and Mn-based additives. CaO, MnO₂, Al₂O₃, ZnO, BaO, PbO, SiO₂, Ba(OH)₂, Ca(OH)₂, CaCO₃, as well as oil soluble Ni, Al, Fe and other compounds [3]. However, in this paper, the effect of a relatively less studied oxide additive, namely CeO₂, on the high temperature corrosion behavior of some superalloys: Superfer 800H (Alloy A), Superco 605 (Alloy B) and Superni 75 (Alloy C), has been investigated in a molten salt environment of Na₂SO₄-60% V₂O₅ under cyclic conditions. Further, the hot corrosion results presented in this paper using CeO₂ inhibitors have been compared with other inhibitors, namely MnO₂, Y₂O₃, SnO₂ and ZrO₂ from the previously published data. The comparison of the hot corrosion behavior of different inhibitors used on the three alloys would provide a useful database for researchers.

EXPERIMENTAL

The Fe-, Ni- and Co-based superalloys under investigation, namely Superfer 800H, Superco 605 and Superni 75, were procured from Mishra Dhatu Nigham Ltd. (MIDHANI), Hyderabad (India). The alloys were in the rolled sheet form with varying thicknesses (1.4–4.0 mm). For convenience, these alloys are designated as A, B and C, respectively, and their chemical compositions are reported in Table 1.

The alloy sheets were cut into rectangular samples of 20 mm x 15 mm. The specimens were polis-

Table 1. Nominal composition of the superalloys used

Alloy Designation	Alloy Midhani Grade (Similar grade)	Chemical Composition (wt.%)									
		Fe	Ni	Co	Cr	Ti	Al	W	Mn	Si	C
A	Superfer 800H (Incoloy 800H)	Bal	32.0	–	21.0	0.3	0.3	–	1.5	1.0	0.1
B	Superco 605 (KC20WN/L 605)	3.0	10.0	Bal	20.0	–	–	15.0	1.5	0.3	0.08
C	Superni 75 (Nimonic 75)	3.0	Bal	–	19.5	0.3	–	–	–	–	0.1

hed down to 1200 grit using silicon carbide papers and finally a cloth wheel polished with the alumina powder (1 μm). These were then washed with distilled water and cleaned with acetone. The physical dimensions of the samples were recorded carefully with a Sylvac digital vernier calliper (resolution 0.01 mm) to evaluate their surface areas. These superalloy samples were exposed to an accelerated corrosion testing in a Silicon Carbide Horizontal Tube Furnace (Digitech) in Na_2SO_4 –60% V_2O_5 , as well as in Na_2SO_4 –60% V_2O_5 + CeO_2 environments for 50 cycles at 900°C. Each cycle consisted of one hour heating in the furnace followed by 20 minutes cooling in the ambient air. The detailed procedure for oxidation studies is reported elsewhere [4, 5], which is reproduced here also for easy understanding.

Before starting the oxidation studies in the furnace, samples were prepared in the following way. For oxidation studies in the Na_2SO_4 –60% V_2O_5 environment, the samples were heated in an oven to a temperature of 250°C, followed by application of a salt mixture of Na_2SO_4 –60% V_2O_5 on all surfaces of all samples with a camel hair brush. The amount of the salt coating varied from 3–5 mg per cm^2 of the surface area of the samples. This salt coating was provided only once at the start of the oxidation studies and no salt was applied during the oxidation studies. These salt coated samples were then dried (~ 110°C) for 2 hours in the oven. Whereas for the Na_2SO_4 –60% V_2O_5 + CeO_2 environment, the samples were first coated with a thin layer of CeO_2 mixed in distilled water (1–2 mg/cm^2) and then heated in the furnace at 900°C for 8 hours to improve the adherence of the coating. A thin layer of Na_2SO_4 –60% V_2O_5 was then applied on these CeO_2 coated warm samples as explained earlier; the total amount of the salt (Na_2SO_4 –60% V_2O_5 + CeO_2) coating ranging up to 5–6 mg/cm^2 . These samples were also dried in the oven for 2–3 hours. This is how the samples were prepared for the cyclic oxidation studies in the furnace [4, 5].

All the prepared samples were subsequently subjected to the accelerated corrosion tests for 50 cycles at 900°C. During the experiment, each sample was kept in an alumina boat and the weight of the boat

and specimen was measured, which was taken as the initial weight for the concerned sample at the start of oxidation cycle number 1. The alumina boats used for the studies were preheated at a constant temperature of 1200°C for 6 h, and it was assumed that their weights would remain constant during the exposure to the high temperature cyclic oxidation in this study. The assumption was confirmed with the help of a pilot experiment on a boat, with the temperature of the experiment being 900°C for 50 cycles. Then the boat containing the sample was inserted into the hot zone of the Silicon Carbide Tube furnace set at 900°C. The furnace was calibrated to an accuracy of $\pm 5^\circ\text{C}$ using Platinum/Platinum-13% Rhodium thermocouple fitted with a temperature indicator of Electromek (Model-1551 P). The holding time in the furnace was one hour in still air at an isothermal temperature of 900°C after which the boat along with the specimen was taken out and cooled at ambient temperature for 20 minutes. At the end of each cycle, the weight of the sample along with the boat (in their original condition) was measured to evaluate the total rate of corrosion. The corrosion products found in the boat, if any, were included in the weight change measurements. However, when sputtering of the scale occurred, the corrosion products went out of the boat, too. All the weight change measurements were taken with an electronic balance having an accuracy of 0.01 mg. The weight change values were plotted with respect to the number of cycles to approximate kinetics of the corrosion. Visual examination of the exposed samples was made after each cycle for their colour, lustre, adherence, spalling tendency and presence/absence of the unreacted salt, etc. [4, 5].

The average oxide scale thickness values of the specimens after exposure at 900°C were obtained from the BSE images of the well polished sectioned samples using Robinson Back Scattered Detector (RBSD) attached with Scanning Electron Microscope (LEO 430VP). For the identification of different phases formed during hot corrosion studies, X-ray diffractometry (XRD) was carried out using Diffractometer PW1140/90 Phillips with the copper target and nickel filter at a voltage of 35kV and a current of 15 mA. Surfaces of the exposed specimens were also

examined using the same Scanning Electron Microscope LEO 435VP. The exposed samples were sectioned with the help of a diamond cutter, mounted and polished for the electron probe micro-analysis (EPMA) using the JXA-8600M microprobe. The mounted samples were carbon coated before performing the EPMA analysis. The elements selected for X-ray mapping were as per the composition of the base sample, type of coating and environment of study [4, 5].

RESULTS

Visual Examination

After the accelerated cyclic hot corrosion in the $\text{Na}_2\text{SO}_4\text{-60\%V}_2\text{O}_5$ environment, the bare alloy A indicated the formation of a dull oxide scale on its surfaces, which was observed to be intact during the initial cycles [4–5]. After cycle number 5, a loose scale was observed at a few places on the surfaces, however, there was no spallation. An marginal amount of spallation started after the 12th cycle and the colour of the scale changed to dark black. There was some more lose of this loose and fragile scale from one corner of the specimen after the 17th cycle. After 50 cycles, the oxide scale was shining black in appearance. For alloy B, the colour of the sample changed from dark brown to dark grey during the first two cycles. The phenomenon of spallation of the oxide scale followed by the fresh scale formation was observed repeatedly throughout the experiment. After 50 cycles, the scale was dull grey with black patches on the surface. Whereas, for alloy C, the colour of the sample changed to silver grey after the 1st cycle. The coating was observed to be adherent till the end of the 12th cycle, with gradual increase in the weight gain, while suddenly spalling occurred during the 13th cycle. After spalling of the scale, the colour of the sample was black. However, there was only a marginal tendency of spallation during the remaining period of the study [4, 5].

After the deposition of the superficial CeO_2 coating, the scale on alloy A showed a grey shining scale. A white coating was visible on the surface till the 15th cycle after that the colour changed to dark black, and spalling started though the amount of the spalled scale was very low. The final scale on alloy B showed black adherent lustrous mass although spalling was continuous after 25 cycles. In case of alloy C, the surface was dull, compact, with whitish and grey areas and black patches indicating the presence of an unreacted thick salt film on the surface of the sample.

Kinetics of High Temperature Corrosion

The weight change data for alloys A, B and C, with and without the CeO_2 coating when exposed to

$\text{Na}_2\text{SO}_4\text{-60\%V}_2\text{O}_5$ at 900°C under cyclic conditions, are presented in Fig. 1. The plot for alloy A with CeO_2 coating shows an increase in the weight gain up to the 20th cycle, then a decreasing trend has been observed up to the 50th cycle. The maximum weight gain is about 7.8 mg/cm² but the final weight after 50 cycles decreased down to 5 mg/cm². In alloy B, a similar trend is observed and in this case the weight also increases up to the 20th cycle and then decreases gradually to about 5 mg/cm². But the maximum weight gain is 15 mg/cm². In case of alloy C, a very slight change is noticed but it is evident from the Figure that an increasing trend is followed up to the 20th cycle, after which it remains nearly constant. Overall weight change is very low, just 1/4th of that without CeO_2 . It may be concluded from the weight change trends that all of the CeO_2 coating were successful to reduce the weight gain of the alloys.

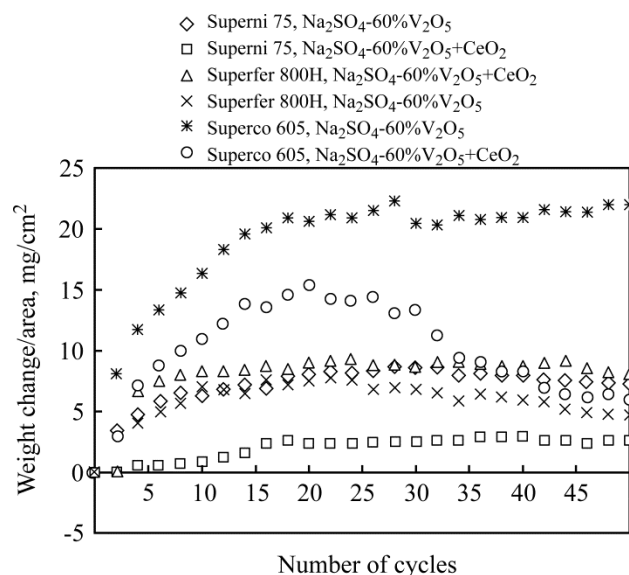


Fig. 1. Weight change vs. number of cycles plots for alloy A (Superfer 800H), alloy B (Superco 605) and alloy C (Superni 75) subjected to cyclic oxidation in $\text{Na}_2\text{SO}_4\text{-60\%V}_2\text{O}_5$ and $\text{Na}_2\text{SO}_4\text{-60\%V}_2\text{O}_5 + \text{CeO}_2$ environments at 900°C for 50 cycles.

X-ray Diffraction Analysis

The XRD data for the $\text{Na}_2\text{SO}_4\text{-60\%V}_2\text{O}_5$ corroded alloys A, B, and C are compiled in Table 2. The prominent phases identified in alloy A are $\alpha\text{-Fe}_2\text{O}_3$, Cr_2O_3 , NiCr_2O_4 , NiFe_2O_4 and FeV_2O_4 . Alloy B has been found to have Cr_2O_3 , NiWO_4 , Co_3O_4 , NiO , CoCr_2O_4 , NiCo_2O_4 and $\text{Co}_3\text{V}_2\text{O}_8$ phases in its scale. In the nickel-based alloy C, the main phases identified are $\text{Ni}(\text{VO}_3)_2$, NiO , Cr_2O_3 and NiCr_2O_4 [4, 5].

Table 3 presents the XRD data for the CeO_2 coated alloys A, B and C exposed to $\text{Na}_2\text{SO}_4\text{-60\%V}_2\text{O}_5$ environment at 900°C for 50 cycles in air. In case of alloy A coated with Ceric oxide in $\text{Na}_2\text{SO}_4\text{-60\%V}_2\text{O}_5$ environment, the main peaks of FeS , Cr_2O_3 , NiCr_2O_4 , NiFe_2O_4 , FeV_2O_4 , Fe_2O_3 and $(\text{Cr, Fe})_2\text{O}_3$ have been identified. In the Co-based alloy B, the main peaks of CoCr_2O_4 and NiCo_2O_4

Table 2. XRD analysis data for the superalloys after exposure for 50 cycles at 900°C in Na₂SO₄-60% V₂O₅ environment [4, 5]

Alloy	"d" Values	Phases Identified
A (Superfer 800H)	2.9558	FeV ₂ O ₄ , NiCr ₂ O ₄
	2.5257	α-Fe ₂ O ₃ , FeV ₂ O ₄ , NiCr ₂ O ₄ , NiFe ₂ O ₄ , Cr ₂ O ₃
	2.1103	α-Fe ₂ O ₃ , FeV ₂ O ₄
	1.7137	α-Fe ₂ O ₃ , FeV ₂ O ₄
	1.6189	FeV ₂ O ₄ , NiCr ₂ O ₄ , NiFe ₂ O ₄ , Cr ₂ O ₃
	1.4864	α-Fe ₂ O ₃ , NiCr ₂ O ₄ , NiFe ₂ O ₄ , Cr ₂ O ₃
	1.2765	α-Fe ₂ O ₃ , Cr ₂ O ₃
	1.0870	α-Fe ₂ O ₃ , Cr ₂ O ₃
B (Superco 605)	3.7035	Cr ₂ O ₃
	2.8996	NiWO ₄ , NiCo ₂ O ₄ , Co ₃ O ₄
	2.4785	NiWO ₄ , Cr ₂ O ₃ , NiCo ₂ O ₄ , CoCr ₂ O ₄
	2.4267	CoO, Co ₃ O ₄ , NiO
	2.1009	CoO, Cr ₂ O ₃ , Co ₃ V ₂ O ₈ , NiO
	2.0555	Co ₃ V ₂ O ₈ , CoO, Cr ₂ O ₃
	1.6732	NiWO ₄ , WO ₃
	1.5808	CoCr ₂ O ₄
	1.4907	CoO, CoCr ₂ O ₄ , NiO
	1.4530	CoO, Co ₃ V ₂ O ₈ , Co ₃ O ₄ , NiCo ₂ O ₄
C (Superni 75)	2.9088	Ni(VO ₃) ₂ , NiCr ₂ O ₄
	2.4785	NiCr ₂ O ₄ , NiFe ₂ O ₄ , Ni(VO ₃) ₂ , Cr ₂ O ₃
	2.3893	NiO
	2.0734	Ni(VO ₃) ₂ , Cr ₂ O ₃
	1.6903	NiFe ₂ O ₄ , Ni(VO ₃) ₂ , Cr ₂ O ₃
	1.5933	NiFe ₂ O ₄ , NiCr ₂ O ₄ , Cr ₂ O ₃ ,
	1.4695	NiCr ₂ O ₄ , Cr ₂ O ₃ , NiO
	1.2606	NiCr ₂ O ₄ , NiO, Cr ₂ O ₃
1.0768	NiCr ₂ O ₄ , Cr ₂ O ₃	

Table 3. XRD analysis of data for the CeO₂ coated superalloys after exposure for 50 cycles at 900°C in Na₂SO₄-60% V₂O₅

Alloy	"d" Values	Phases Identified
A (Superfer 800H)	3.6145	αFe ₂ O ₃ , (Cr, Fe) ₂ O ₃ , Cr ₂ O ₃
	2.9181	FeV ₂ O ₄ , Fe ₂ O ₃ , FeS
	2.6641	(Cr, Fe) ₂ O ₃ , Cr ₂ O ₃ , FeS
	2.4918	NiCr ₂ O ₄ , NiFe ₂ O ₄ , FeV ₂ O ₄ , Fe ₂ O ₃ ,
	2.3893	(Cr, Fe) ₂ O ₃
	2.0644	NiO
	1.8220	FeS, NiO, Cr ₂ O ₃
	1.6903	FeV ₂ O ₄ , (Cr, Fe) ₂ O ₃
	1.6009	(Cr, Fe) ₂ O ₃ , FeV ₂ O ₄ , FeS
	1.4695	NiCr ₂ O ₄ , NiFe ₂ O ₄ , (Cr, Fe) ₂ O ₃ , Fe ₂ O ₃ , Cr ₂ O ₃
	1.4490	NiCr ₂ O ₄ , NiFe ₂ O ₄ , FeV ₂ O ₄ , Fe ₂ O ₃ , Cr ₂ O ₃
1.2677	(Cr, Fe) ₂ O ₃ FeV ₂ O ₄	
B (Superco 605)	3.7035	WO ₃ , CoWO ₄
	2.8996	Co ₃ O ₄ , NiCo ₂ O ₄ , NiWO ₄ , CoWO ₄
	2.4785	NiCo ₂ O ₄ , NiWO ₄ , Co ₃ O ₄ , CoCr ₂ O ₄ , CoO, Cr ₂ O ₃
	2.3651	NiO
	2.1009	Co ₃ V ₂ O ₈ , WO ₃ , CoO, NiO
	2.04665	NiCo ₂ O ₄ , WO ₃ , Cr ₂ O ₃ , NiO
	1.6817	NiWO ₄ ,
	1.5833	Co ₂ O ₃ , CoCr ₂ O ₄ , Cr ₂ O ₃
	1.4907	WO ₃ , CoCr ₂ O ₄ , CoO
	1.4530	NiCo ₂ O ₄ , Co ₃ O ₄ , Cr ₂ O ₃
C (Superni 75)	3.1828	CeO ₂
	2.9751	Ni(VO ₃) ₂ , NiS
	2.7111	CeO ₂ , CeVO ₄ , Cr ₂ O ₃
	2.5465	Ni(VO ₃) ₂ , NiCr ₂ O ₄ , NiO, NiS
	2.4267	NiO, Ni(VO ₃) ₂ , Cr ₂ O ₃
	2.0917	NiO, Ni(VO ₃) ₂ , Cr ₂ O ₃
	1.9119	CeO ₂ , CeVO ₄ , NiS
	1.6401	CeO ₂ , Cr ₂ O ₃
	1.4779	NiO, NiCr ₂ O ₄ , Cr ₂ O ₃
	1.2080	NiCr ₂ O ₄ , NiO, Cr ₂ O ₃
	1.1045	NiCr ₂ O ₄ , NiO

have been identified and other possible phases may be WO_3 , CoWO_4 , Co_3O_4 , Cr_2O_3 , NiWO_4 and $\text{Co}_3\text{V}_2\text{O}_8$. In the Ni-based alloy C (Superni 75), the main phase identified is NiO. Whereas CeO_2 may possibly be present along with other phases such as NiS, Cr_2O_3 , NiCr_2O_4 and $\text{Ni}(\text{VO}_3)_2$.

Scale Thickness Measurements

Oxide scale thickness values after exposure to the Na_2SO_4 -60% V_2O_5 environment at 900°C in air for 50 cycles were measured from the back scattered images for alloys A, B, and C. The scale was having maximum thickness in the case of alloy B and minimum in alloy C; the values measured were 63, 78 and 39 μm for alloys A, B, and C, respectively [4, 5]. Whereas, the average thickness values for the scales of the CeO_2 coated alloys A, B and C were 50, 42, 25 μm , respectively. Evidently, the oxide scale thicknesses have reduced after the deposition of the CeO_2 coating.

SEM Analysis

In alloy A in Fig. 2a, there is a massive scale showing craters and the presence of some crystalline phases on the top surface of the scale. The surface Energy Dispersive X-Ray Analysis (EDAX) of the same alloy in Fig. 3a and Table 4, corresponding to different points on the scale surface, indicates the presence of Fe, Ni and Cr in the scale. Ceric oxide is randomly distributed at some points in the scale. In area 2, where mainly CeO_2 is present, Ni is absent but Fe and Cr are present though in smaller amounts. In case of alloy B, the SEM micrograph in Fig. 2b and the SEM/EDAX analysis at the points marked in Fig. 4, corresponding to this alloy and given in Table 5, both indicate the formation of nodules of the Co-rich phase containing mainly Co, Cr and a low amount of Fe. V is present in the scale surface at all points, with chromium and cobalt at points 1 and 3, whereas at point 2, 46% of V is present with 69% of ceric oxide. The SEM micrograph for alloy C in Fig. 2c shows that the scale consists of a matrix having coarse grains with nodules across the scale. The SEM morphologies for alloys A, B, and C, exposed to the Na_2SO_4 -60% V_2O_5 induced corrosion without any additive, have been reported in the earlier publication of the authors [4].

EPMA and SEM/EDAX Analyses

In case of alloy A, the EPMA results shown in Fig. 5 indicate the formation of a thick dense scale which consists mainly of Cr, Ni and some Fe. A thin layer above the interface is poor in Ni and Cr but rich in Fe; in the areas depleted of Fe silicon is present in a higher concentration throughout the scale. The EDAX analysis of the alloy across the scale

shown in Fig. 3 and Table 4 indicates an outer scale rich in Fe and containing Cr and Ni. Ceric oxide is indicated as trace element near the substrate scale interface. Internal oxidation is indicated where mainly Ti is oxidized along the grain boundaries. V is present throughout the scale.

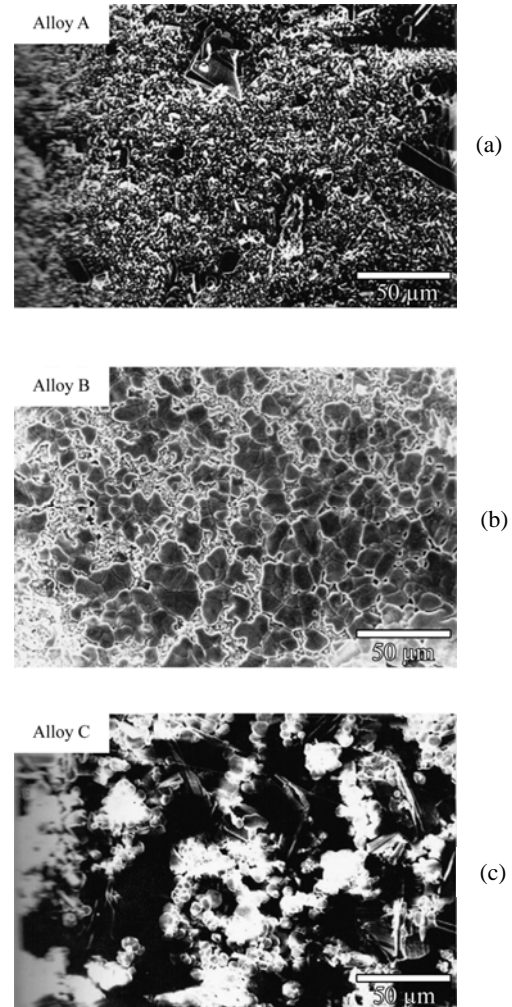


Fig. 2. SEM micrographs showing the surface morphology of alloy A (Superfer 800H), alloy B (Superco 605) and alloy C (Superni 75) subjected to cyclic oxidation at 900°C for 50 cycles in Na_2SO_4 -60% V_2O_5 + CeO_2 environment.

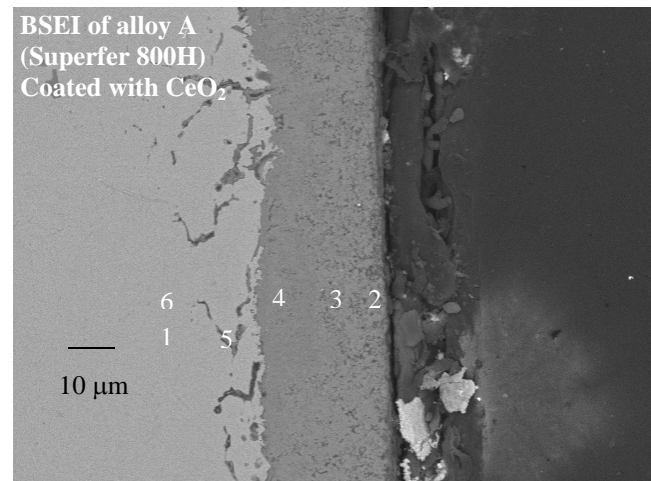
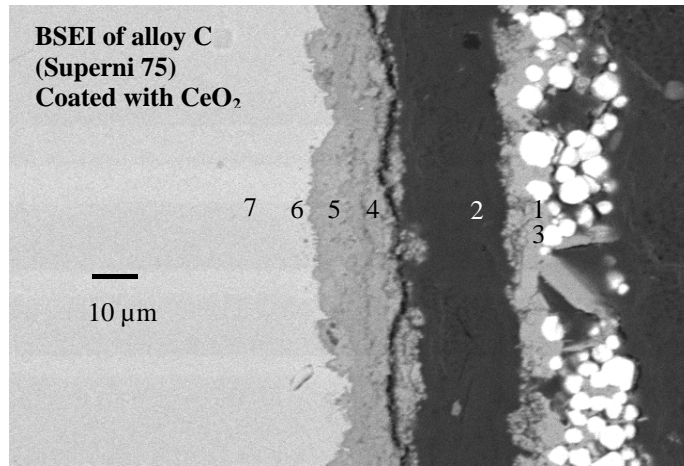


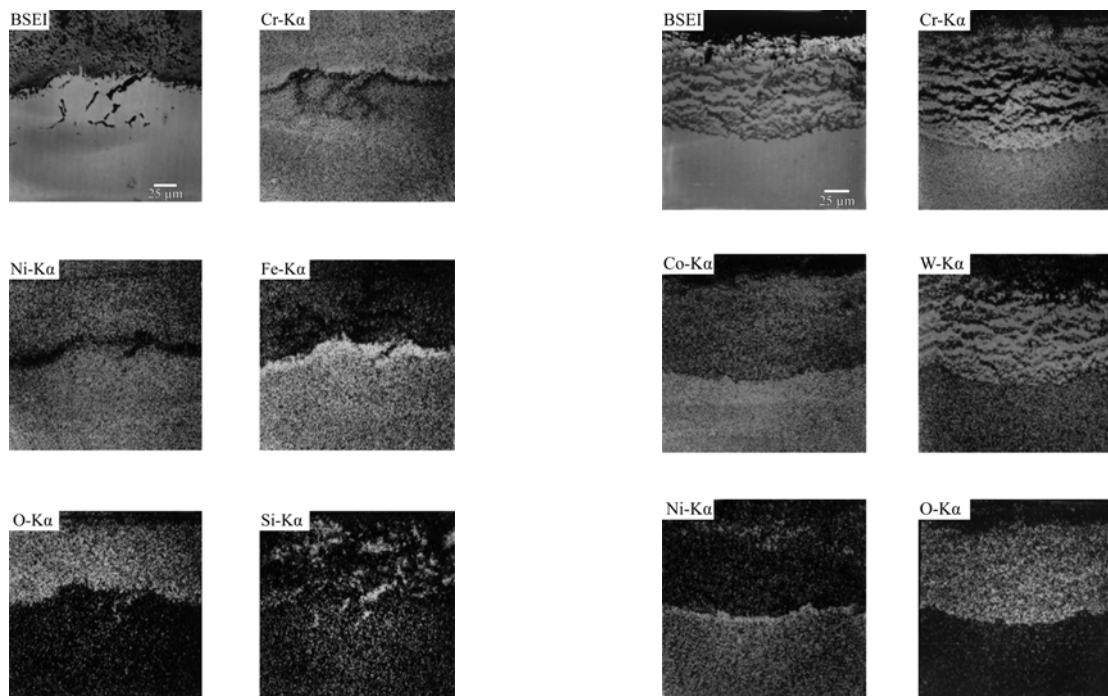
Fig. 3. Back scattered image of alloy A (Superfer 800H) after cyclic hot corrosion in Na_2SO_4 -60% V_2O_5 + CeO_2 at 900°C .

Table 4. Wt. % of elements corresponding to points marked in Fig. 3, BSE image of alloy A (Superfer 800H)

Point of Analysis	Weight % of Elements										
	O	Cr	Fe	Ni	Mn	Ti	Al	Si	V	Na	Ce
1	35	17	33	13	1	1	0.22	1	–	–	–
2	32	15	31	18	1	–	0.13	2	2	–	–
3	32	19	36	10	1	1	0.11	–	1	0.05	–
4	31	24	32	11	1	1	–	–	1	–	0.06
5	24	18	23	15	1	10	2.65	5	–	0.01	–
6	0	12	42	44	–	1	0.11	1	–	–	0.06

**Fig. 4.** Back scattered image of alloy C (Superni 75) after cyclic hot corrosion in Na_2SO_4 -60% V_2O_5 + CeO_2 at 900°C.**Table 5.** Wt. % of elements corresponding to points marked in Fig. 4, BSE image of alloy C (Superni 75)

Point of Analysis	Weight % of Elements						
	O	Cr	Fe	Ni	Ti	Ce	V
1	24	–	–	1	–	74	1
2	24	8	–	66	–	2	1
3	18	5	–	22	–	51	4
4	28	35	1	36	1	–	1
5	28	26	–	45	1	–	1
6	26	23	–	51	–	–	–
7	–	17	–	83	–	–	–

**Fig. 5.** BSEI and X-ray mappings of the cross-section of alloy A (Superfer 800H) subjected to cyclic oxidation at 900°C for 50 cycles in Na_2SO_4 -60% V_2O_5 + CeO_2 environment.**Fig. 6.** BSEI and X-ray mappings of the cross-section of alloy B (Superco 605) subjected to cyclic oxidation at 900°C for 50 cycles in Na_2SO_4 -60% V_2O_5 + CeO_2 environment.

The EPMA analysis for alloy B, Fig. 6, indicates a thick dense scale consisting mainly of Cr and Co. Ni is present in smaller amounts where Cr is absent, Co is present in a high concentration throughout the scale. There is no internal oxidation indicated. There is a thin layer all along the alloy/scale interface rich in nickel. Oxygen is present throughout the scale.

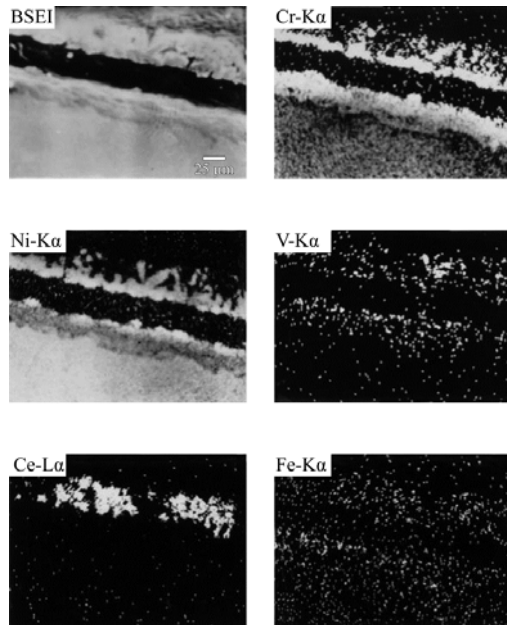


Fig. 7. BSEI and X-ray mappings of the cross-section of alloy C (Superni 75) subjected to cyclic oxidation at 900°C for 50 cycles in $\text{Na}_2\text{SO}_4\text{-60\%V}_2\text{O}_5 + \text{CeO}_2$ environment.

The EPMA of alloy C, Fig. 7, indicates the formation of a scale consisting mainly of Ni and Cr. There is indication of the growth of crystals rich in Ni-Cr, which suggests the spinel formation. Ceric oxide is present in a high concentration in the scale and at same places it is co-existing with V. The bottom of the scale contains mainly Cr and Ni. V is present in both the top and bottom layers.

The EDAX analysis along the cross-section of alloy C, coated with CeO_2 exposed to $\text{Na}_2\text{SO}_4\text{-60\%V}_2\text{O}_5$ at 900°C shown in Fig. 4 and Table 5, indicates the presence of the unreacted ceric oxide on the top surface as point 1 shows the presence of mainly Ce and oxygen. Vanadium is present all along the cross-section. The inner scale contains mostly oxides of Ni and Cr. Ti is also present throughout the cross-section along with Ni, Cr, and oxygen. Fe is present in the scale though in small amounts.

The EPMA analysis for the bare alloys corroded in the $\text{Na}_2\text{SO}_4\text{-60\%V}_2\text{O}_5$ environment at 900°C for 50 cycles has been reported elsewhere [4].

DISCUSSION

In the studied environment the maximum weight gain was observed in alloy B and minimum in alloy C. The sequence of hot corrosion rates based on the overall weight gain after 30 cycles is as follows:

Alloy B > Alloy A > Alloy C.

The superior resistance of Ni-based alloys to the given environment is, perhaps, due to the formation of a protective layer of Cr_2O_3 and of nickel vanadate. The same has been reported by Kerby and Wilson [6] in their study on the Ni- and Fe-based alloys in $\text{Na}_2\text{SO}_4\text{-V}_2\text{O}_5$. A detailed discussion on the hot corrosion of these alloys has been reported in the earlier publication of the authors [4].

In case of the CeO_2 coated samples, a thick scale is observed in alloys A and B, whereas it is of a medium size in alloy C. The scale thickness values are 50, 42, 25 μm for alloys A, B, and C, respectively. But there is an indication of reduction in the rate of corrosion for all of the alloys. The weight gain has also decreased to some extent in all of the alloys. This decrease is 23% in alloy A, 35% in alloy B, and 68% in alloy C. Thus it can be inferred that ceric oxide is effective in case of all alloys but it is most effective in alloy C.

A thick dense scale mainly containing Cr, Ni and Fe is indicated in alloy A (Fig. 5). There is penetration of the scale into the substrate where mainly Si is getting oxidized along the grain boundaries. Such findings have also been reported by Roy et al. [7] in their study on the superficially ceric-oxide-coated AISI-347 grade stainless steel. The internal oxidation of silicon along the alloy grain boundaries and formation of such phases have been also reported in [7]. Roy and co-authors have observed Si concentrated at the alloy/oxide interface and the Si-rich subscale well extended as stringers into the underlying alloy along the grain boundaries. The XRD pattern from the outer surface of the scale formed reveals the formation of NiCr_2O_4 , FeV_2O_4 , Fe_2O_3 , Cr_2O_3 , and $(\text{Cr, Fe})_2\text{O}_3$. The EDAX of the surface and cross-section has indicated the presence of ceric oxide in the scale, even though the EPMA analysis failed to detect it probably due to its low concentration. The inhibiting effect of the superficially applied CeO_2 in the aggressive environment of $\text{Na}_2\text{SO}_4\text{-60\%V}_2\text{O}_5$ may be due to the presence of ceric oxide in the scale and a thin continuous layer of Cr_2O_3 present at the margin of the scale, abounding the substrate and thus impeding the transport of species.

In case of alloy B, the maximum weight change is nearly 1/3rd of that without ceric oxide in $\text{Na}_2\text{SO}_4\text{-60\%V}_2\text{O}_5$. Cobalt, tungsten and chromium are seen in the scale. But W is mainly present in the form of elongated streaks where Cr is absent, which indicates a stepwise formation of a scale where first Cr gets oxidized, and in the Cr-depleted area below it the concentration of W increases, so W gets oxidized and then just beneath this concentration of Cr increases and so it also gets oxidized. The thus-formed Cr_2O_3 may be responsible for lowering the

Table 6. Reactions of Ceric oxide with vanadium compounds [9]

	Conditions of Reaction	Reaction
1	50 m/o CeO ₂ -Na ₃ VO ₄ for 54h at 700°C	No reaction
2	35 m/o CeO ₂ -NaVO ₃ for 92h at 700°C	No reaction
3	66 m/o CeO ₂ in V ₂ O ₅ in 2h at 700°C,	2CeO ₂ + V ₂ O ₅ = 2CeVO ₄ + 1/2 O ₂
4	40 m/o CeO ₂ - 20 m/o V ₂ O ₅ - 40 m/o NaVO ₃ heated for 24h at 700°C	CeVO ₄ was formed
5	50 m/o CeO ₂ - 25 m/o V ₂ O ₅ - 25 m/o Na ₂ SO ₄ heated for 17h under air at 700°C	V ₂ O ₅ reacted preferentially with CeO ₂ .
6	35 m/o CeO ₂ in NaVO ₃ and	Producing CeVO ₄ .
7	20 m/o CeO ₂ - 38 m/o NaVO ₃ - 42 m/o Na ₂ SO ₄ under 50 ± 10 Pa of SO ₃ in air at 700°C	CeO ₂ + NaVO ₃ (in Na ₂ SO ₄) + SO ₃ = CeVO ₄

While CeO₂ and NaVO₃ do not react directly, CeO₂ is converted to CeVO₄ if V₂O₅ is produced in the melt by the reaction of NaVO₃ and SO₃.

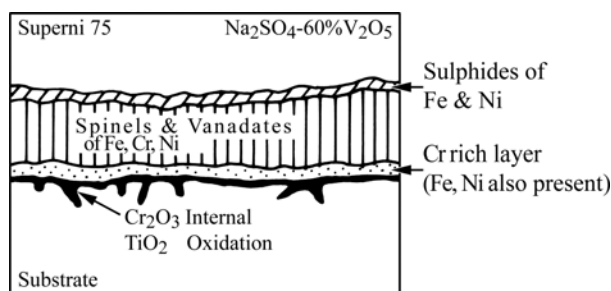


Fig. 8. Schematic of the oxide scale for alloy C (Superni 75) subjected to cyclic oxidation in Na₂SO₄-60%V₂O₅ environment at 900°C for 50 cycles.

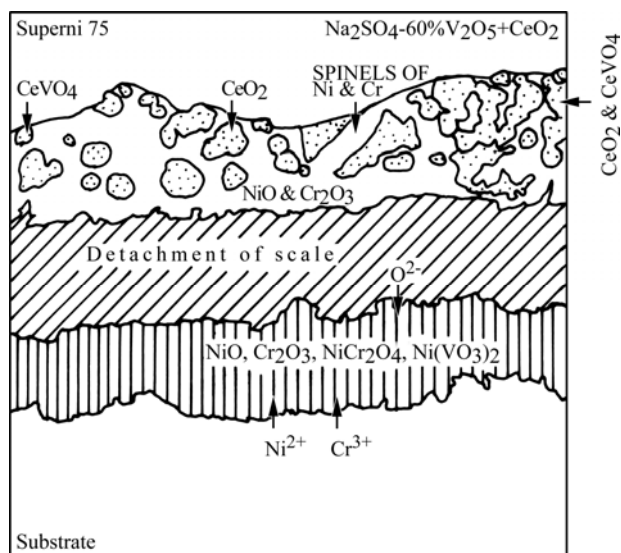


Fig. 9. Schematic of the oxide scale for alloy C (Superni 75) subjected to cyclic oxidation in Na₂SO₄-60%V₂O₅ + CeO₂ environment at 900°C for 50 cycles.

extent of corrosion. The XRD also indicates the presence of CoCr₂O₄, NiCo₂O₄, Co₂O₃, Co₃O₄, Cr₂O₃, and NiWO₄ compounds on the surface scale after the hot corrosion run.

In alloy C, a thick Cr₂O₃ continuous layer has been observed in EPMA, which is, perhaps, contributing to decreased corrosion rates. The formation of CeVO₄ may be suggested at places where Ce and V are co-existing. The presence of CeO₂ in alloy C is indicated by the XRD analysis, where the formation of CeVO₄ is also established from the EPMA micrographs. Thus the presence of CeO₂ on the surface and possibly the formation of CeVO₄ may be contributing to the reduction of the corrosion attack

in alloy C. Reidy and Jones [8] have suggested that ceric oxide is chemically inert to the molten NaVO₃-SO₃ system at 1073K for the SO₃ partial pressure up to 3×10^{-6} atm. But at a higher SO₃ partial pressure, CeO₂ with V₂O₅ components of the melt react to form CeVO₄. The conditions of the reaction are captured in Table 6 as reported by Jones et al. [9] Further, Ecer et al. [10] in their study have reported that the rates of oxidation of both the Ni- and Fe-based alloys were markedly reduced by the superficial application of CeO₂ powder on the alloy surface and also the scale adherence was improved, which resulted in marked changes in the oxidation morphology. Seal and co-authors in [11] and [12]

Table 7. Comparison of results of different inhibitors used on the three superalloys (Alloy A, Alloy B and Alloy C)
 * (After 30 Cycles) mg/cm^2 † (After 50 cycles in most of the alloys) μm

Environment	Alloy	*Weight Change	†Scale Thickness	XRD	SEM/EDAX/EPMA
Na ₂ SO ₄ -60% V ₂ O ₅ [4]	A	8.77	62.5	α -Fe ₂ O ₃ , FeV ₂ O ₄ , NiCr ₂ O ₄ , NiFe ₂ O ₄ , Cr ₂ O ₃	Cavities visible on the surface showing spalled regions, a thick scale having horizontal cracks, and the top layer rich in Ni and Fe. A discontinuous Cr-rich layer is present near the scale/substrate interface. A nickel-rich continuous layer is present just above the substrate.
	B	20.34	78	NiWO ₄ , Cr ₂ O ₃ , NiCo ₂ O ₄ , CoCr ₂ O ₄ , Co ₃ O ₄ , NiO, CoO, Co ₃ V ₂ O ₈	A thick multilayer scale is formed, consisting of the Fe- and Ni-rich scale at the top, which also contains Co and Cr. A thick layer having W follows it, containing Fe and Cr. But the areas rich in W are poor in Cr. The Cr-rich subscale is present just above the interface. Vanadium is distributed throughout the scale. A higher concentration of S is indicated just above the substrate where Mn is also present in a higher concentration indicating the MnS formation just below the W-rich scale.
	C	8.34	38.5	NiCr ₂ O ₄ , NiO, NiFe ₂ O ₄ , Ni(VO ₃) ₂ , Cr ₂ O ₃	A medium size scale shows a Cr-rich layer near the substrate, V is present throughout the scale. Ti present as a thin irregular layer above the substrate and S at the top. The Cr-rich layer is just above the substrate. In this area, Ni and Fe are also occurring with Cr. V is also indicated in the scale and V is occurring in the layer, just above the substrate where Ni, Fe and Cr are present.
Na ₂ SO ₄ -60% V ₂ O ₅ +CeO ₂	A	6.78	50	NiCr ₂ O ₄ , Cr ₂ O ₃ , NiFe ₂ O ₄ , FeS, FeV ₂ O ₄ , Fe ₂ O ₃ and (Cr, Fe) ₂ O ₃	A massive scale showing craters and presence of some crystalline phases is revealed by SEM. EDAX of the surface scale shows the presence of Fe, Ni and Cr. Ceric oxide is randomly distributed at some points in the scale. EDAX of the cross-section also reveals that the top scale is rich in Fe and contains Cr and Ni. Ceric oxide is indicated as trace element. EPMA shows a thin continuous layer of Cr ₂ O ₃ present at the margin of the scale. The scale mainly consists of Cr, Ni and some Fe. Si has got oxidized along the grain boundaries.
	B	13.23	41.5	NiCo ₂ O ₄ , NiWO ₄ , Co ₃ O ₄ , CoCr ₂ O ₄ , CoO, Cr ₂ O ₃ , NiO	The surface EDAX indicates nodules of the Cr-rich phase containing mainly Co, Cr, a little amount of Ceric oxide, etc. V is seen at some places in the matrix, present in large concentration with Ceric oxide. EPMA revealed a thick dense scale mainly consisting of Cr and Co. Co is present in a high concentration throughout the scale and the internal oxidation is indicated.
	C	2.66	25	NiO, FeS, NiCr ₂ O ₄ , Ni(VO ₃) ₂ and CeO ₂	A SEM micrograph for alloy C shows that the scale consists of a matrix having coarse grains with nodules across the scale. EPMA reveals the growth of Ni-Cr rich crystals indicating the spinel formation. Ceric oxide is present in a high concentration in the scale and at same places it is co-existing with V indicating a probable formation of CeVO ₄ .
Na ₂ SO ₄ -60% V ₂ O ₅ +MnO ₂ [15]	A	7.37	30	FeV ₂ O ₄ , Fe ₂ O ₃ , FeS, NiCr ₂ O ₄ , NiFe ₂ O ₄ , and NiCrMnO ₄	SEM indicated a massive scale formation. The EPMA indicates formation of a medium size scale, which is mainly rich in iron at the top. Al and S are also present in the outer scale. The scale just above the substrate is Cr-rich where Ni and Mn are absent. Penetration of the scale into the substrate due to the internal oxidation of Cr is indicated. Ti is also present in the scale just above the substrate/scale interface.

	B	13.47	53.5	Co ₃ O ₄ , Co ₃ V ₂ O ₈ , NiCo ₂ O ₄ , Cr ₂ O ₃ , CoO, NiWO ₄ , Co ₂ MnO ₄	Two distinct layers are seen in SEM, the upper layer indicates partial melting but the inner scale is dense. EPMA indicated a thick scale consisting mainly of W, Cr, Fe and a little amount of Ni. Wherever W is present, areas are Cr-depleted. There is a nickel-rich layer at the interface; S is present in the outermost scale and also as a thin layer along the interface between the scale and the substrate. MnS is located near the interface. The EDAX analysis reveals also the presence of Co, Cr and W in the outermost scale. At the alloy/substrate interface the amount of W is lower and the amount of Cr is higher. The presence of Na, V and S, as well as of Mn, is indicated along the cross-section of the scale.
	C	5.35	20.5	NiCr ₂ O ₄ , Ni(VO ₃) ₂ , NiS, NiCrMnO ₄ , NiO, Mn ₃ O ₄ , Cr ₂ O ₃ , Fe ₂ O ₃	There is a large-sized crystal growth in alloy C. The scale is relatively thin and consists mainly of Cr with some amount of Ni and Ti. The layer beneath the Cr-rich scale is rich in Ni but poor in Cr. Mn and V are co-existing throughout the scale. The outer scale above the Cr ₂ O ₃ scale is rich in Fe.
Na ₂ SO ₄ -60%V ₂ O ₅ +Y ₂ O ₃ [5]	A	1.15	20	FeV ₂ O ₄ , Fe ₂ O ₃ , Cr ₂ O ₃ , FeS, CrS, Y ₂ O ₃	SEM shows the presence of sulphurous compound. A thin scale is formed that has a band rich in Cr, which is continuous. The presence of an unreacted salt is indicated on the surface of the sample. MnS is present in the substrate. Y is co-existing with V in the scale, indicating a possible formation of YVO ₄ .
	B	7.40	30	Co ₃ V ₂ O ₈ , Cr ₂ O ₃ , NiWO ₄ , NiCo ₂ O ₄ , Co ₃ O ₄ , Cr ₂ O ₃ and CoCr ₂ O ₄	The spongy scale observed from the SEM micrograph having pores indicates the release of some gas or vapour. EPMA shows that the scale is rich in chromium and cobalt. EDAX of the cross-section reveals the presence of Y in the scale at some spots where V is also present in a higher concentration indicating the formation of YVO ₄ . The scale just above the substrate is Cr-depleted.
	C	3.39	16.5	NiCr ₂ O ₄ , NiO, NiS, Cr ₂ O ₃ , NiCr ₂ S ₄ , TiO ₂ and Y ₂ O ₃	SEM indicates unreacted salt crystals. A thin scale is observed that contains mainly Cr and Ni. Y is present as a thin layer along with V and S on the top of the scale.
Na ₂ SO ₄ -60%V ₂ O ₅ +SnO ₂ [16]	A	7.26	32	Fe ₂ O ₃ , FeV ₂ O ₄ , NiCr ₂ O ₄ , NiFe ₂ O ₄ , Cr ₂ O ₃ , FeS, (Cr, Fe) ₂ O ₃ and SnO ₂	A thick scale is formed and on the top of this scale the unreacted SnO ₂ is seen. The scale mainly contains Fe and Cr as revealed by their respective X-ray images. There is a thin Cr-rich continuous band above the substrate. The presence of SnO ₂ is even obvious from the crystalline growth observed by the SEM analysis of the top surface of the scale. The presence of this refractory SnO ₂ on the scale is possibly helpful in decreasing the rate of corrosion
	B	6.96	52	Co ₂ O ₃ , Co ₃ O ₄ , Co ₃ V ₂ O ₈ , CoCr ₂ O ₄ , NiCr ₂ O ₄ , NiWO ₄	SEM indicates a massive scale with intergranular cracks and irregular shaped craters in the scale. The medium size scale is formed mainly consisting of Co. Cr that is present in the top layer in the W-depleted areas and a band type Cr-rich thick layer present above the substrate. S is indicated at the top of the scale and sulphide specks seen near the interface. Presence of MnS is indicated at the interface between the substrate and scale.
	C	4.21	34	SnO ₂ , Cr ₂ O ₃ and NiO	SEM indicates crystalline phase indicating SnO ₂ presence on the surface. Elemental X-ray mapping reveals that the scale is mainly containing Cr and lesser amount of Ni. Sn is present in higher concentration at top of the scale where as V is present in the main scale indicating formation of nickel vanadates.

Na ₂ SO ₄ - 60%V ₂ O ₅ + ZrO ₂ [4]	A	7.83	43	Fe ₂ O ₃ , ZrO ₂ , FeV ₂ O ₄ , NiFe ₂ O ₄ , Cr ₂ O ₃ , NiO, (Cr, Fe) ₂ O ₃ , NiCr ₂ O ₄	Crystalline and globular structure is being revealed by SEM. EDAX showed that the scale is rich in iron and contains Cr, Ni and Zr with V and S. As we proceed inwards, it remains basically Fe-rich scale and V is seen across the scale. S also penetrates up to the substrate. Internal oxidation is indicated. EPMA confirms the presence of Cr, Ni, and Fe in the scale. V and Zr are also present in the scale. Ni enrichment is observed along the alloy/scale interface. Al and Ti are also there in the scale.
	B	10.94	58	CO ₃ O ₄ , CO ₃ V ₂ O ₈ , Co ₂ NiO ₄ , CoCr ₂ O ₄ and NiWO ₄	Trans-granular cracks and granular structure indicating some porosity in the grains is observed in the scanning electron micrograph. BSEI and X-ray images showed the formation of a thick scale having distinct layers. The top layer is rich in chromium and Co followed by the middle layer, rich in W and where W is present but Co is absent. The inner layer is Cr rich. Nickel is also present in the upper layer and areas rich in Ni are poor in Cr.
	C	2.51	17.5	ZrO ₂ , Cr ₂ O ₃ & NiCr ₂ O ₄	A dense scale with large size nodules which on higher magnification show the crystal growth with directionality indicating oxidation of inter-metallic phases. EPMA shows a very thin scale mainly consisting of chromium and iron and some patches with a higher concentration of S. V is incorporated in the scale as well as a small amount of Zirconium.

have also reported that superficially applied CeO₂ not only reduced the rates of scale growth for all of the three varieties of steel but also imparted an improved scale adhesion to the respective alloy substrates. Similar reporting has also been made by Mitra et al. [13] in their study on the superficially applied CeO₂ coating on the 304 stainless steel. They assumed that such improvement could be due to the change in the mechanism of the scale growth from the scale/gas interface to the alloy/scale interface and faster attainment of the steady state Cr₂O₃-rich scale along with the complex spinel formation. Schematic representation of the corrosion mechanism for the superficially coated ceria in case of alloy C is shown in Fig. 8.

The main reason for reducing the attack of the corrosive environment in alloy C may be the presence of an unreacted CeO₂ on the surface. The presence of the Cr₂O₃ layer in the scale and of the very highly concentrated Cr₂O₃ thin layer above the substrate/scale interface may also be a contributing factor for the protection of those alloys. The CeO₂ coated alloy B, i.e. Superco 605, gave the thinnest scale (see Fig. 9). The presence of the Cr₂O₃ thin layer near the substrate may be contributing to lowering the extent of corrosion. Ceria has been identified on the top of the scale in alloys A and B by the SEM/EDAX analysis. The presence of ceria might have also led to better adhesion of the scale and affected the scale growth mechanism. Internal oxidation of silicon in alloy A has been observed by EPMA; these internal oxide stringers may be contributing to better adhesion of the scale. A similar

observation has also been reported by Roy et al. [14]. The formation of CeVO₄ could not be confirmed by XRD whereas both Ce and V are co-existing in the scale of all the alloys. A comparison of results of the hot corrosion behavior of the three superalloys (Alloy A, B, and C) using different inhibitors is given in Table 7. The data presented in that Table were published in the previous works elsewhere [4, 5, 15–16].

CONCLUSIONS

The deposition of the CeO₂ coating on the superalloys A (Superfer 800H), B (Superco 605) and C (Superni 75) led to the decrease in corrosion rates during the first 30 cycles. The scale thickness values also indicate that this additive could be effective in providing protection to the alloys in the aggressive environment of Na₂SO₄-60%V₂O₅.

On the basis of the total weight gain measurements (around 30 cycles), the following conclusions can be drawn:

- In Na₂SO₄-60%V₂O₅, the corrosion rate is significant and follows the trend Alloy B > Alloy A > Alloy C.
- CeO₂ is most effective in alloy C where it has reduced the weight gain to about 1/3. In the other two alloys the extent of inhibition is lower, but nearly the same in both.
- When the Ceric oxide is a superficial coating, the main reasons for reducing the attack of the corrosive environment in alloy C may be the presence of the unreacted CeO₂ on the surface. The presence

of the Cr₂O₃ layer in the scale and of the very highly concentrated Cr₂O₃ thin layer above the substrate/scale interface may also be a contributing factor for the protection of these alloys.

- A better inhibiting behavior of alloy B may also be ascribed to the band type Cr-rich thick layer present just above the substrate.

- Among the superalloys, alloy C, i.e. Superni 75, gave the best resistance to the attack by Na₂SO₄-60%V₂O₅; and nearly all the inhibitors, in particular, CeO₂, SnO₂, ZrO₂, and Y₂O₃ are most effective for inhibiting the hot corrosion in the above environment. The Superco-605, Alloy B, has been found to have the lowest resistance to the given environment; also, in it the inhibiting effect is comparatively lower with all inhibitors used.

- The most beneficial effect of superficial coatings of CeO₂, Y₂O₃, SnO₂ and ZrO₂ is a considerable improvement in the scale adherence to the alloy substrate as minimum spalling was observed with these coatings, and even the coating remained intact in most of superficially coated samples, which has been confirmed by visual observations.

REFERENCES

1. Rapp R.A., Zhang Y.S. Hot Corrosion of Materials: Fundamental Studies. *JOM*. 1994, **46**(12), 47–55.
2. Rapp R.A. Hot Corrosion of Materials. *Pure & Appl Chem*. 1990, **62**(1), 113–22.
3. Paul L.D. and Seeley R.R. Oil Ash Corrosion – A Review of Utility Boiler Experience. *Corrosion*. 1991, **47**(2), 152–59.
4. Gitanjaly, Singh H., Prakash S. Effect of Superficially Applied ZrO₂ Inhibitor on the High Temperature Corrosion Performance of Some Fe-, Co- and Ni-base Superalloys. *Appl Surf Sci*. 2008, **254**(20), 6653–6661.
5. Gitanjaly, Singh H., Prakash S. High Temperature Corrosion Behavior of Some Fe-, Co- and Ni-base Superalloys in the Presence of Y₂O₃ as Inhibitor. *Appl Surf Sci*. 2009, **255**, 7062–7069.
6. Kerby R.C., Wilson J.R. Corrosion of Metals by Liquid Vanadium Pentoxide and the Sodium Vanadates. *J Eng Power*. 1973, **95**(1), 36–44.
7. Roy S.K., Bottino C., Rakesh V.R., Kuiry S.C., Bose S.K. Improved High Temperature Oxidation Behavior of AISI 347 Grade Stainless Steel by Superficial Coating of CeO₂. *ISIJ Int*. 1995, **35**(4), 433–442.
8. Reidy R.F., Jones R.L. Thermogravimetric Analysis of the Reaction of CeO₂ with the NaVO₃-SO₃ System. *J Electrochem Soc*. 1995, **142**(4), 1352–1356.
9. Jones R.L., Williams C.E. Hot Corrosion of Co-Cr-Al-Y by Molten Sulfate-Vanadate Deposits. *Mater Sci Eng*. 1987, **87**, 353–360.
10. Ecer G.M., Singh R.B., Meier G.H. The Influence of Superficially Applied Oxide Powders on the High-temperature Oxidation Behavior of Cr₂O₃ Forming Alloys. *Oxid. Met.* 1982, **18**(1/2), 55–81.
11. Seal S., Bose S.K., Roy S.K. Improvement in the Oxidation Behavior of Austenitic Stainless Steels by Superficially Applied Cerium Oxide Coatings. *Oxid. Met.* 1994, **41**(1/2), 139–178.
12. Seal S., Roy S.K., Bose S.K., Kuiry S.C. Ceria-based High-temperature Coatings for Oxidation Prevention, *JOM-e*, 2001, 1. <http://www.tms.org/pubs/journals/JOM/0001/Seal/Seal-0001.html>.
13. Mitra S.K., Roy S.K., Bose S.K. Influence of Superficial Coating of CeO₂ Oxidation Behavior of AISI 304 Stainless Steel. *Oxid Met.* 1993, **39**(3/4), 221–229.
14. Roy S.K., Bottino C., Rakesh V.R., Kuiry S.C. and Bose S.K. Improved High Temperature Oxidation Behavior of AISI 347 Grade Stainless Steel by Superficial Coating of CeO₂. *ISIJ Int.*, 1995, **35**(4), 433–442.
15. Gitanjaly, Bala N., Singh H. and Prakash S. Effect of MnO₂ Additions on the Hot Corrosion Behavior of Some Fe-, Co- and Ni-base Superalloys. *Proc. Material Science and Technology (MS&T) 2007 Conference and Exposition: Energy*. September 16–20, 2007, 53–66.
16. Goyal G., Bala N., Singh H., Prakash S. Role of Superficially Applied SnO₂ Inhibitor in Controlling High Temperature Corrosion of Some Fe-, Co- and Ni-base superalloys. *Oxid Met.* 2014, **82**(1/2), 49–69.

Received 21.01.14

Accepted 02.06.14

Реферат

Коррозионные свойства металлов и сплавов при высоких температурах могут быть модифицированы с использованием ингибиторов. В настоящей работе исследовано влияние нанесенных покрытий из CeO₂ на поверхность суперсплавов, таких как Superfer 800H (сплав А), Superco 605 (сплав В) и Superni 75 (сплав С) с целью предотвращения высокотемпературной коррозии. Ускоренные коррозионные испытания суперсплавов с покрытиями и без них были выполнены в солевом расплаве Na₂SO₄-60%V₂O₅ при 900°C в течение 50 циклов. Анализ оксидных пленок на испытанных образцах был выполнен с применением методов оценки потери веса, рентгеноструктурного анализа, сканирующей электронной микроскопии, энергодисперсионной спектроскопии. Прирост массы на сплавах А, В и С с нанесенным покрытием CeO₂ был меньше на 23, 35 и 68% соответственно. Следовательно, применение оксида церия наиболее эффективно для уменьшения скорости коррозии сплава С.

Ключевые слова: жаропрочные сплавы, высокотемпературная коррозия, ингибиторы, добавки оксидов.